Molecular and Cellular Neuroscience 88 (2018) 308–318

Contents lists available at ScienceDirect

Molecular and Cellular Neuroscience

journal homepage: www.elsevier.com/locate/ymcne

24S-hydroxycholesterol suppresses neuromuscular transmission in SOD1(G93A) mice: A possible role of NO and lipid rafts

Kamilla A. Mukhutdinova[a], Marat R. Kasimov[a], Arthur R. Giniatullin[a], Guzel F. Zakyrjanova[a,b], Alexey M. Petrov[a,b,*]

[a] Institute of Neuroscience, Kazan State Medial University, Butlerova st. 49, Kazan 420012, Russia
[b] Laboratory of Biophysics of Synaptic Processes, Kazan Institute of Biochemistry and Biophysics, Federal Research Center "Kazan Scientific Center of RAS", P. O. Box 30, Lobachevsky St., 2/31, Kazan 420111, Russia

ARTICLE INFO

Keywords:
24S-hydroxycholesterol
Amyotrophic lateral sclerosis
Neuromuscular junction
Synaptic vesicle
Exocytosis
Nitric oxide
Lipid rafts

ABSTRACT

Amyotrophic lateral sclerosis (ALS) is a neurodegenerative disorder characterized by the initial denervation of skeletal muscle and subsequent death of motor neurons. A dying-back pattern of ALS suggests a crucial role for neuromuscular junction dysfunction. In the present study, microelectrode recording of postsynaptic currents and optical detection of synaptic vesicle traffic (FM1-43 dye) and intracellular NO levels (DAF-FM DA) were used to examine the effect of the major brain-derived cholesterol metabolite 24S-hydroxycholesterol (24S-HC, 0.4 μM) on neuromuscular transmission in the diaphragm of transgenic mice carrying a mutant superoxide dismutase 1 (SOD^{G93A}). We found that 24S-HC suppressed spontaneous neurotransmitter release and neurotransmitter exocytosis during high-frequency stimulation. The latter was accompanied by a decrease in both the rate of synaptic vesicle recycling and activity-dependent enhancement of NO production. Inhibition of NO synthase with L-NAME also attenuated synaptic vesicle exocytosis during high-frequency stimulation and completely abolished the effect of 24S-HC itself. Of note, 24S-HC enhanced the labeling of synaptic membranes with B-subunit of cholera toxin, suggesting an increase in lipid ordering. Lipid raft-disrupting agents (methyl-β-cyclodextrin, sphingomyelinase) prevented the action of 24S-HC on both lipid raft marker labeling and NO synthesis. Together, these experiments indicate that 24S-HC is able to suppress the exocytotic release of neurotransmitter in response to intense activity via a NO/lipid raft-dependent pathway in the neuromuscular junctions of SOD^{G93A} mice.

1. Introduction

A disturbance in synaptic communication lies at the heart of many neurodegenerative diseases and pharmacological approaches that act on the synaptic level are sought as a potential strategy for treatments. Amyotrophic Lateral Sclerosis (ALS) is a fatal disease leading to the progressive loss of both upper and lower motor neurons. Transgenic mice expressing a mutant copper/zinc superoxide dismutase 1 (SOD) gene develop a motor neuron disease resembling human ALS and they are commonly used as models for it (Gurney et al., 1994; Narai et al., 2009; Duplan et al., 2010; Gordon et al., 2010; Cappello et al., 2012; Rocha et al., 2013; Nascimento et al., 2015). Studies of SOD^{G93A} mice show a pattern of dying-back pathology (Nijssen et al., 2017). The earlier event in the ALS represents a denervation of neuromuscular junctions (NMJs) that occurs before the death of motor neurons (Fischer et al., 2004; Narai et al., 2009). Histological and electrophysiological studies reveal a similar pattern in ALS patients (Fischer et al., 2004; Nijssen et al., 2017). Together, these results suggest that NMJs are particularly vulnerable to damage in the progression of ALS, and suggest that this finally leads to diaphragm paralysis and respiratory failure, causing death. Early changes in neurotransmitter release were revealed at the NMJs in soleus muscle of SOD^{G37R} mice and in the diaphragms of SOD^{G93A} mice (Naumenko et al., 2011; Rocha et al., 2013; Nascimento et al., 2015; Arbour et al., 2015). In addition, a dysfunction of some proteins engaged in synaptic vesicle recycling and a reduction of the total size of the synaptic vesicle pool may be involved in ALS pathology (Cappello et al., 2012; Liu et al., 2015; Coyne et al., 2017).

ALS has also been found to be associated with marked changes in lipid metabolism, including cholesterol homeostasis (Wuolikainen et al., 2014; La Marca et al., 2016; Abdel-Khalik et al., 2017). According to some studies, hyperlipidemia is directly correlated with better survival in patients with ALS and lowering the levels of plasma cholesterol by statins may accelerate the disease progression (Dupuis et al., 2008;

* Corresponding author at: P. O. Box 30, 2/31 Lobachevsky St., Kazan Institute of Biochemistry and Biophysics, Kazan, Russia.
E-mail address: aleksey.petrov@kazangmu.ru (A.M. Petrov).

https://doi.org/10.1016/j.mcn.2018.03.006
Received 7 November 2017; Received in revised form 8 February 2018; Accepted 12 March 2018
Available online 14 March 2018
1044-7431/

Zheng et al., 2013). Dyslipidemia and hypercholesterolemia may be accompanied by elevated plasma level of 24S-hydroxycholesterol (24S-HC), a major brain-derived cholesterol metabolite (Leoni and Caccia, 2013; Dumolt et al., 2017). In contrast to the CNS, where the concentration of 24S-HC varies in the range 10–30 μM (Lütjohann et al., 1996), the total plasma level of 24S-HC is about 0.2 μM, or 80 ng/ml in healthy volunteers (Babiker and Diczfalusy, 1998; Leoni and Caccia, 2013). The concentrations found in mouse plasma are lower than in human ranging from about 6 to 25 ng/ml in mice (Shafaati et al., 2010; Crick et al., 2015). Plasma level of 24S-HC may be significantly changed in some pathological conditions in a stage-dependent manner (Meng et al., 1997; Leoni and Caccia, 2013). In patients with some forms of neurodegeneration, an enhancement of 24S-HC production occurs in the early stage of the disease and then its synthesis is markedly reduced during the progressive neuronal loss (Leoni and Caccia, 2013; Petrov et al., 2017a). This may explain some discrepancies in measurements of 24S-HC. Wuolikainen et al. (2014) found that the plasma concentration of 24S-HC was increased (from 62 to 71 ng/ml) in females with ALS. By contrast, other studies revealed reduced levels of 24S-HC in cerebrospinal fluid and plasma (from 89 to 42 ng/ml) of ALS patients (La Marca et al., 2016; Abdel-Khalik et al., 2017).

Our recent study revealed that 24S-HC, at submicromolar range, could enhance synaptic vesicle cycling and affect retrograde NO signaling at the mouse NMJs (Kasimov et al., 2017). Given the dying-back pattern of pathology, early disturbance of NMJ functionality, respiratory dysfunction, and a potential implication of 24S-HC in the progression of ALS, it seems interesting to study the effect of 24S-HC on synaptic transmission in the diaphragm of SOD^{G93A} mice. Here, we report that 24S-HC (0.4 μM) suppresses both spontaneous release and evoked release during intense activity. The latter is dependent on both a decrease in the rate of synaptic vesicle retrieval and attenuation of activity-induced NO signaling via a lipid raft-dependent mechanism.

2. Methods

2.1. Ethical approval

This investigation conforms to the Guide for the Care and Use of Laboratory Animals (NIH Publication No. 85–23, revised 1996) and European Convention for the Protection of Vertebrate Animals used for Experimental and other Scientific Purposes (Council of Europe No 123, Strasbourg, 1985). Experiments were performed on the isolated diaphragm muscle of SOD^{G93A} transgenic mice at the symptomatic disease stage (Gurney et al., 1994), characterized by paralysis of the hind limbs (6–7 months of age). Mice transgenic for the $SOD1^{G93A}$ mutation on a B6SJL background (B6SJL-Tg(SOD1-G93A)dl1Gur/J strain; purchased from The Jackson Laboratory) that harbor the mutated allele of the human SOD1 gene were maintained as a hemizygous line in an SPF-breeding facility (Branch of Shemyakin and Ovchinnikov Institute of Bioorganic Chemistry, Pushino). The onset of the disease phenotype is delayed compared to the original high copy number strain (SOD1 G93A)1Gur, due to a decrease in transgenic copy number. Age-matched outbred B6/SJL mice, referred to as wild-type (WT), were used for comparison; they were exposed to the same conditions as the $SOD1^{G93A}$ mice. Mice had free access to food and water and were maintained in a 12-h light/12-h dark cycle.

Both male and female mice were used in equal proportions. Experiments without (control) and with application of 24S-HC were performed in tandem on both hemidiaphragms. Animals were anesthetized by an intraperitoneal injection of sodium pentobarbital (40 mg/kg) before decapitation with a guillotine. The chest was then immediately opened and the muscle quickly excised. The experimental protocol met the requirements of the EU Directive 2010/63/EU and was approved by the Bioethics Committees of Kazan Medical University.

2.2. Bathing solution and chemicals

Hemidiaphragms with a phrenic nerve were attached to the bottom of a Sylgard-lined chamber (volume, 5 ml), which was superfused at 5 $ml \cdot min^{-1}$ throughout the experiment with mammalian physiological saline containing (in mM): NaCl-129.0, KCl-5.0, $CaCl_2$-2.0, $MgSO_4$-1.0, NaH_2PO_4-1.0, $NaHCO_3$-20.0, glucose-11.0 and HEPES-3.0. The solution was saturated with a 5% CO_2 and 95% O_2 mixture to maintain pH. Experiments were performed at 24–25 °C which allows the muscle to maintain a stable level of neurotransmitter release for a long period (Glavinović, 1979) and to prevent rapid leakage of fluorescent dye (DAF-FM) from the cytosol (Pye et al., 2007). The phrenic nerve was stimulated with a suction electrode connected to an extracellular stimulator (DS3 Digitimer Ltd., UK) by supramaximal electrical pulses of 0.1 ms duration. In some experiments (electrophysiology and FM1-43/DAF-FM fluorescence), the muscle fibers were cut transversely to prevent muscle contractions and to simultaneously maintain the physiological level of quantal release of acetylcholine.

24S-HC (Enzo Life Sciences) was dissolved in DMSO (the final concentration of DMSO in the working solution did not exceed 0.001%). The concentration of 24S-HC was 0.4 μM, which is sufficient to evoke a submaximal effect on synaptic vesicle exocytosis at the NMJs of WT mice (Kasimov et al., 2017). Preparations were treated with 0.4 μM 24S-HC for 15 min before high-frequency stimulation. DMSO (0.001%) by itself did not alter any of the measured parameters (spontaneous or evoked postsynaptic currents; labeling with FM1-43, DAF-FM and CTxB), consistent with our previous observation (Kasimov et al., 2017). Therefore the data from DMSO controls were pooled together with DMSO-free controls.

Nω-nitro-L-arginine methyl ester hydrochloride (100 μM L-NAME, an inhibitor of NO synthase) was added to the external solution 30 min before 24S-HC treatment and remained in the bath throughout the experiment. In some experiments, we used a 10 min treatment with methyl-β-cyclodextrin (MβCD, 0.1 mM) or sphingomyelinase (SMase, 0.1 μ/ml; from *Staphylococcus aureus*, Sigma) to disrupt lipid rafts. Under these conditions, MβCD or SMase was added after 15 min application of 24S-HC. The osmolarity of the solution was adjusted when the reagents were added to physiological solution.

2.3. Electrophysiology

Recording of postsynaptic end-plate currents (EPCs) and miniature EPC (MEPCs) was performed using standard two-electrode voltage clamp technique with intracellular glass microelectrodes (tip diameter ~1 μm, resistance 3-5MΩ, filled with 2.5 M KCl). The junctional zone was located between two microelectrodes separated by distance of ~200–300 μm. The holding potential for the cut muscle fibers was kept at −45 mV (leak current in the range of 10–30 nA, ≤10% of EPC amplitudes). The motor nerve was stimulated by single (1 stimulus in 20 s) or high-frequency trains (20 Hz) of suprathreshold pulses. The recorded signals were digitized at 50 kHz and analyzed off-line using PC software. Recording instrumentation consisted of an Axoclamp 900 A (Molecular devices, USA) amplifier and LA II digital I/O board (Pushino, Russia) under the control of locally written software.

2.4. Fluorescence microscopy

Fluorescence images were acquired using an Olympus BX51WI microscope with a confocal attachment Disk Speed Unit and LumPlanPF 100 × w objective. Images were captured with DP71 CCD camera (Olympus). Image analysis was performed using CellˆP (Olympus) and ImagePro software (Media Cybernetics, Bethesda, MD, USA). Multiple z axis optical sections were taken using a focus stepper (ECO-MOT). Intensity analysis was made on regions of interest in arbitrary units (a.u.), which were then converted into percentages. Only nerve terminals on surface muscle fibers were studied. All dyes were from

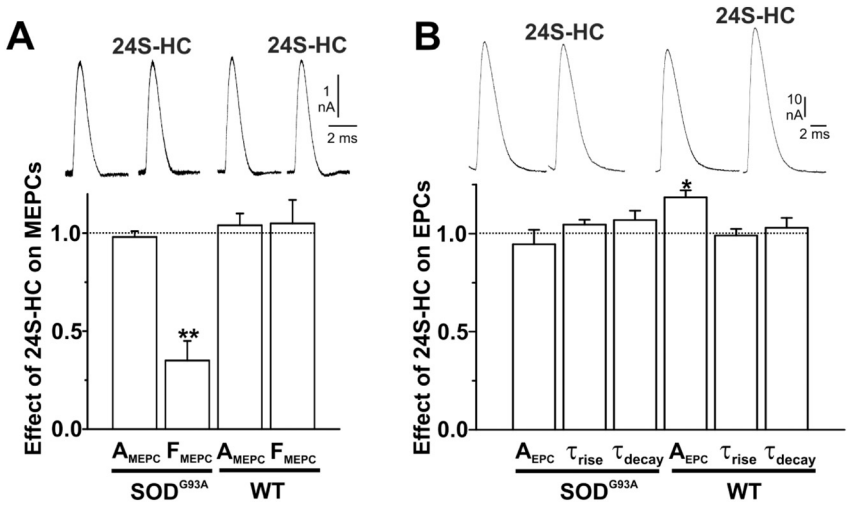

Fig. 1. Influence of 24S-HC on spontaneous and evoked neurotransmitter release in SOD^{G93A} and WT mice. Top, typical MEPCs/EPCs before and 15 min after treatment with 24S-HC. A/B - Histograms showing the effect of 24S-HC on peak amplitude (A_{MEPC}) and frequency (F_{MEPC}) of MEPCs/on parameters of EPCs (amplitude - A_{EPC}; rise time - τ_{rise}, decay time -τ_{decay}). EPCs were elicited at 0.05 Hz. The ordinates show the normalized effect of 24S-HC (1.0 – is the value prior to 24S-HC application). Asterisks denote significant differences (*P < 0.05; **P < 0.01).

Molecular Probes.

2.5. Loading and unloading of FM1-43

The fluorescent dye FM1-43 was used for tracking the rate of exocytosis. FM1-43 reversibly binds to the surface membranes and becomes loaded in the synaptic vesicles during endocytosis. Trains of 20 Hz stimulation for 1 min were used to load FM1-43 into the nerve terminals. The dye (5 μM) was present in the bath during and 5 min after stimulation. The muscles were then washed with physiological saline containing ADVASEP-7 (3 μM) for 15 min to accelerate dissociation of FM1-43 from the plasma membranes and to decrease non-specific staining. The phrenic nerve was re-stimulated at 20 Hz to induce synaptic vesicle exocytosis, which leads to a decrease in fluorescence of the nerve terminals (dye unloading). For estimating the effect on exocytosis, drug application was performed after ADVASEP-7 perfusion. To record FM1-43 fluorescence intensity we used a 480/20 nm excitation filter, a 505 nm dichroic mirror and a 535/40 nm emission filter. Background fluorescence was estimated as the mean fluorescence intensity in an area ($4 \times 20\,\mu m^2$) outside of the nerve terminal. Nerve terminal fluorescence intensity was defined as the average pixel intensity in regions of interest, drawn manually, after subtraction of background fluorescence. For analysis of the kinetics of unloading, the value of the initial nerve terminal fluorescence (before stimulation) was taken as 1.0.

2.6. Estimation of recycling time

FM1-43 unloading curves give an indication of the number of synaptic vesicles that release FM1-43 by exocytosis. After the exocytotic events, both neurotransmitter and FM1-43 are lost from the fused vesicles and newly formed vesicles contain little or no dye. Exocytosis of recycled vesicles during continued stimulation will produce neurotransmitter release, but no decrease in FM1-43 fluorescence. The cumulative EPC amplitude curves indicate the amount of neurotransmitter released due to all exocytotic events. Superposition of the scaled inverted FM1-43-loss curve and the summed EPC amplitude curve allows us to estimate the mean time of synaptic vesicle recycling (Reid et al., 1999; Rizzoli and Betz, 2005). This time is determined by the point of divergence of the curves, i.e. when the rate of FM-1-43 destaining begins to delay compared to the rate of acetylcholine release.

2.7. Measurements of nitric oxide (II)

Products of NO oxidation were detected using a DAF-FM-diacetate, which was excited with 495/10 nm light. To detect DAF-FM fluorescence, an emission filter that transmits light between 505 and 560 nm was used. The isolated muscles were incubated for 20 min with 4 μM DAF-FM-diacetate. After exposure to the dye, the hemidiaphragms were perfused with physiological solution for 40–50 min and then measurements of the fluorescence in the junctional region were performed.

2.8. Labeling of lipid rafts

Ganglioside GM1, a well-established lipid raft component, was visualized after staining using Alexa Fluor 488-labeled cholera toxin subunit B (CTxB), which is pentavalent for ganglioside GM1. The hemidiaphragms were incubated for 20 min in physiological solution with CTxB (1 μg/ml). The muscles were then washed for 30 min and visualized. Treatment with 24S-CH occurred before CT-B staining. Fluorescence was defined as the averaged fluorescence from pixels in junctional membrane regions. Postsynaptic acetylcholine receptors were labeled by exposing the preparation to 30 ng/ml of rhodamine-conjugated α-bungarotoxin (Btx) for 20 min simultaneously with CTxB. CT-B and Btx fluorescence was excited by light of 480/15 nm and 555/15 nm wavelength; emission was recorded using band-pass filters 505–545 and 610–650 nm, respectively.

2.9. Statistical analysis

Statistical analysis was performed using Origin Pro 9.2 software (OriginLab Corp.), assuming a significance level of 0.05. The results of the experiments are presented as Mean ± S.E.M., where n is the number of independent experiments on different animals, with statistical significance assessed by the Student's *t*-test or repeated one–way ANOVA (for parametric data) followed by the Bonferroni post-hoc test and Mann-Whitney test (for non-parametric data).

3. Results

3.1. Spontaneous and evoked neurotransmitter release

MEPCs were recorded prior to and during application of 0.4 μM 24S-HC. No significant changes in the MEPC amplitude, rise- or decay time were observed. However, 24S-HC significantly decreased MEPC frequency ($1.78 \pm 0.33\,s^{-1}$ before and $0.63 \pm 0.18\,s^{-1}$ after 24S-HC, $P < 0.01$, paired t-test, n = 6 animals) in $SOD1^{G93A}$ mice (Fig. 1A). In control experiments without 24S-HC application, the frequency of MEPCs was relatively stable ($1.81 \pm 0.25\,s^{-1}$ and after 15 min $1.76 \pm 0.26\,s^{-1}$; n = 6 $SOD1^{G93A}$ mice). On the other hand, under conditions of low-frequency stimulation, the oxysterol had no

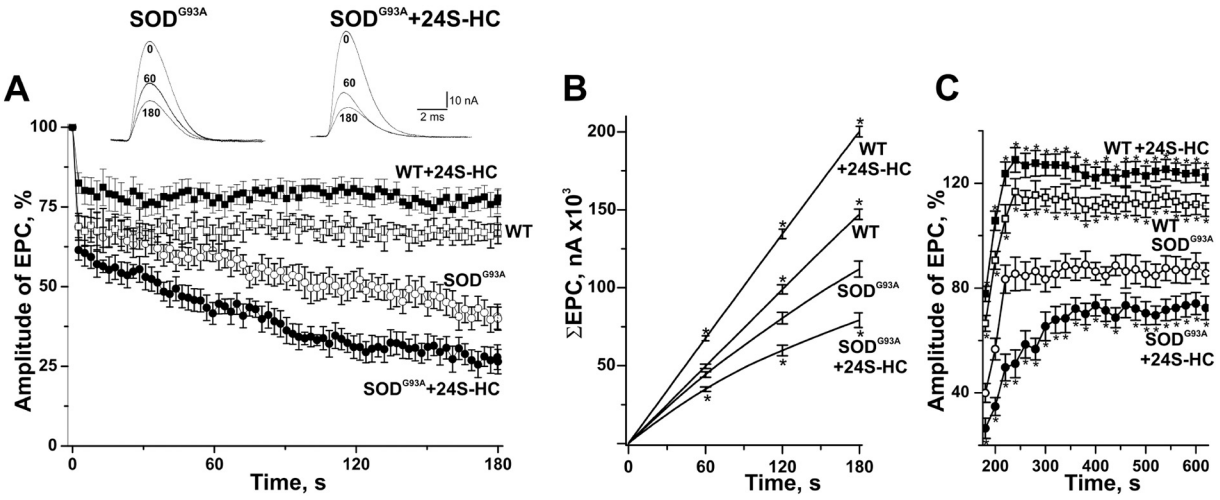

Fig. 2. 24S-HC-mediated changes in synaptic transmission during and after high frequency stimulation. A- Depression of EPC amplitude (in %) during 20 Hz-stimulation of the phrenic nerve in 24S-HC-treated/non-treated SOD^{G93A} mice and wild-type (WT) mice. Top, representative EPCs at 0, 60, 180 s of 20 Hz stimulation. B- Cumulative curves of the EPC amplitudes (from A; in nA) during 3 min 20 Hz-stimulus train. Differences in the curve slopes suggest that pretreatment with 24S-HC suppressed neurotransmitter release induced by high-frequency activity in SOD^{G93A} mice. C- Recovery of the EPC amplitude after the 3 min 20 Hz-train. X-axis begins from 180 s, when the 20 Hz-stimulation was completed. A, C - Data are expressed as percent change from the initial value before 20 Hz stimulation. B,C- *Asterisks display significant differences ($P < 0.05$) versus corresponding value in SOD^{G93A} mice.

significant influence on EPC amplitude ($P < 0.05$ paired t-test, n = 6 animals), rise- and decay-time in SOD1^{G93A} mice (Fig. 1B). These data suggest that 24S-HS suppressed spontaneous neurotransmitter release, without affecting evoked release in response to a single stimulus at the NMJ of ALS model mice. In contrast, in WT mice 24S-HC enhanced the evoked neurotransmitter release at 0.05 Hz stimulation ($P < 0.05$, n = 6 animals), without changing the frequency of spontaneous exocytosis (n = 6 animals) (Fig. 1). It should be noted that at rest, the frequency of MEPCs was similar in WT ($1.45 \pm 0.41\ s^{-1}$, n = 8 animals) and SOD1^{G93A} mice.

Activation of the motor nerve at low frequency provokes exocytosis of only a small part of the synaptic vesicle pool docked at the active zone. High-frequency prolonged stimulation leads to recruitment of additional synaptic vesicles to neurotransmitter release. Under these conditions the maintenance of release is dependent on delivery of the vesicles to the active zone and their reuse (Rizzoli and Betz, 2005; Slater, 2015). A biphasic dynamic of EPC amplitude (comprising an initial rapid decline and a “plateau” at a level of 65–70% of the pre-stimulation value; $P < 0.001$, n = 8 animals) was observed during 3 min of 20 Hz-stimulation at the NMJs of WT mice (Fig. 2A). In contrast, in SOD^{G93A} mice this stimulation resulted in a 3-step change in the EPC amplitude: a rapid drop followed by a 30 s-plateau and then a slower decline to 39.9 ± 3.6% ($P < 0.001$, n = 7 animals) by the 3rd min of the stimulus train. After treatment with 24S-HC, the plateau phase disappeared at the NMJs of SOD1^{G93A} mice, and after the initial rapid decline the EPC amplitude continued to drop (with a slower rate) to 26.5 ± 3.8% ($P < 0.001$, n = 8 animals) by the 3rd min of stimulation (Fig. 2A). Since the MEPC amplitude was unchanged by 24S-HC, summation of the EPC amplitudes during 3 min 20 Hz stimulation provides an estimation of cumulative evoked neurotransmitter release. Pre-treatment with 24S-HC significantly decreased the summed EPC amplitude by 29.3 ± 4.2% ($P < 0.05$) in SOD1^{G93A} mice. Thus, 24S-HC increased the rate of synaptic depression during prolonged 20 Hz-stimulation, leading to a reduction in the cumulative acetylcholine release in NMJs of ALS model mice (Fig. 2B). In contrast, in WT mice 24S-HC had the opposite effect on the rate of the synaptic depression and total transmitter release in response to high frequency stimulation (Fig. 2A, B; n = 8 animals). Note that the summed EPC amplitude was lower by 23.9 ± 3.5% ($P < 0.05$) at the NMJs of SOD1^{G93A} mice compared with that of WT mice.

In addition, SOD^{G93A} mice showed an impairment of recovery of the EPC amplitude after a 20-Hz stimulus train. The amplitude reached only 85.4 ± 6.4% ($P < 0.05$, n = 7 animals) 1 min after the end of 20 Hz stimulation, while post-tetanic potentiation of the EPC amplitude was detected at the NMJs of WT mice (n = 7 animals). Treatment with 24S-HC interfered further with the EPC amplitude recovery in the SOD^{G93A} mice, with the amplitude reaching only 51.1 ± 5.3% ($P < 0.05$, n = 7 animals) by 1 min after the end of 20 Hz-stimulation (Fig. 2C). This suggests that application of 24S-HC may aggravate the impairment of post-tetanic potentiation in the NMJs of SOD^{G93A} mice. In contrast, in WT mice the recovery of the EPC amplitude was slightly accelerated by 24S-HC (n = 7 animals). To exclude any change in the size of the quanta or/and the sensitivity of postsynaptic receptors to acetylcholine, we recorded the MEPCs immediately before and at the end of 20 Hz stimulus train. No significant changes in the mean MEPC amplitude were revealed in any experimental group (Suppl. 1).

It should be noted that for the electrophysiological experiments, NMJs of SOD^{G93A} mice characterized by relatively high amplitude of EPCs were chosen for recording. These NMJs had an initial quantal content which is similar to that of WT mice.

3.2. FM1-43 loading and unloading. Estimation of vesicle recycling time

FM1-43 was loaded into nerve terminals by 1-min stimulation at 20 Hz. The mean value of FM1-43 fluorescence at the NMJs of SOD^{G93A} mice (n = 25 animals) was similar to that of WT mice (n = 24 animals), but a distribution of the fluorescence values was markedly different (Fig. 3A). In SOD^{G93A} mice, NMJs could be divided into two groups characterized by high (I) and low (II) FM1-43 loading. A close to normal distribution of the fluorescence intensities was observed in WT-mice.

After a 1-h rest period, the NMJs loaded with FM1-43 were re-stimulated at 20 Hz to detect dye release due to synaptic vesicle exocytosis (Fig. 3B, C). In WT mice, 24S-HC markedly accelerated the rate of FM1-43 loss (n = 8 animals) compared to non-treated controls (n = 9 animals). In SOD^{G93A} mice, a rapid FM1-43 unloading occurred in the NMJs with the initially high fluorescence (n = 7 animals; group I; Fig. 3B), whereas slow FM1-43-destaining kinetics were observed in the NMJs with the initially low FM1-43 loading (n = 5 animals; group II; Fig. 3C). Treatment with 24S-HC did not modify the nerve terminal fluorescence at rest (Suppl. 2), but it reduced the rate of FM1-43 loss during high frequency stimulation in both groups of NMJs (n = 6/7 animals for group I/II). Surprisingly, this effect of 24S-HC was clearly expressed only after the first 1–2 min of 20 Hz stimulation, and the initial phase of the FM1-43 unloading did not differ between the treated

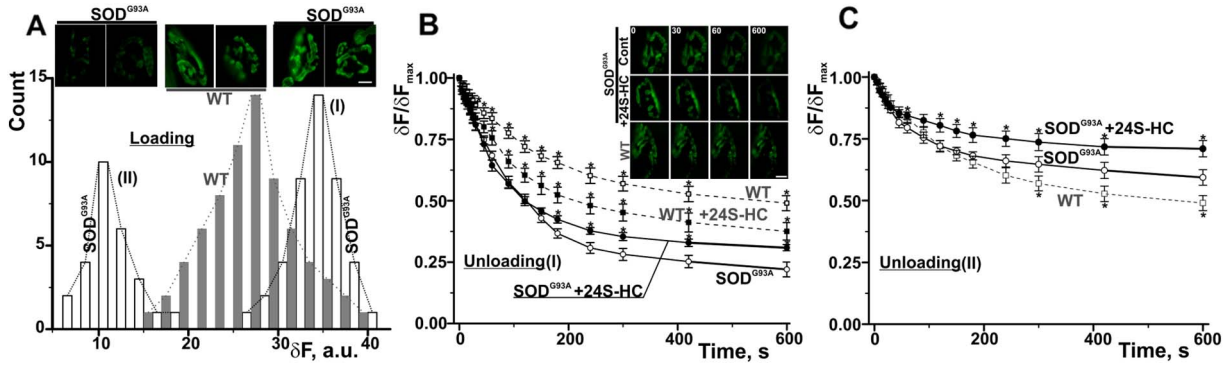

Fig. 3. Exo-endocytosis in the motor nerve terminals: effects of 24S-HC. A – Distribution of values of nerve terminal fluorescence in SOD^{G93A} and WT mice. The FM1-43 was loaded into the nerve terminals by 20 Hz stimulation for 1 min. Top, fluorescent images of the FM dye-loaded NMJs. X-axis – fluorescence intensity (δF) in a.u.; bin size is 2 a.u. for each bar. Y-axis – number of NMJs with the corresponding mean fluorescence ("Count"). In contrast to WT mice, in SOD^{G93A} mice there are two groups of the NMJs characterized by higher (I) and lower (II) FM1-43 uptake. B/C – FM1-43 unloading curves in response to prolonged 20 Hz stimulation determined in the NMJs of SOD^{G93A} mice with initially high (I group)/low (II group) fluorescence. The control unloading curve (WT mice) is shown in B/C as thin dashed curve. In addition, effect of 24S-HC in WT mice is shown in B. Y-axis, normalized fluorescence intensity (δF/δFmax), relative to the value before the onset of the 20 Hz stimulation. B, top – the fluorescent images of NMJs immediately prior to 20 Hz train (0) and at different times (in s) during the stimulus train. A, B - scale bars – 10 μm.

and non-treated NMJs of SOD^{G93A} mice (Fig. 3B, C). This gives rise to a discrepancy because the FM-dye loss in the first minute of the stimulation was not changed by 24S-HC, while the neurotransmitter release was markedly suppressed at the same time in SOD^{G93A} mice (Fig. 2A, B). Comparison of the inverted unloading curve and the cumulative EPC curve (see Methods) suggests that 24S-HC might increase or decrease the time required for the synaptic vesicle recycling in SOD^{G93A} and WT mice, respectively (Fig. 4). Taken together, these data suggest that slower vesicle recycling suppresses neurotransmitter release during the first minutes of 20 Hz activity in 24S-HC-treated NMJs of SOD^{G93A} mice.

It should be noted that the estimated recycling time in the NMJs characterized by high initial FM1-43 loading and fast dye unloading profile (group I) was about the same as in WT mice (Fig. 4). These data suggest that the enhanced depression of neurotransmitter release during high-frequency activity in SOD^{G93A} mice (Fig. 2A,C) may be explained by a reduction in the size of the synaptic vesicle pool that is involved in recycling during intense activity without changing the rate of vesicle recycling.

3.3. Involvement of NO in the effect of 24S-HC on synaptic vesicle exocytosis

Recently, we have found that 24S-HC modulates synaptic vesicle cycling during high-frequency activity by attenuating NO-dependent signaling at the NMJs of WT mice (Kasimov et al., 2017). To estimate the activity-induced changes in NO synthesis at the NMJs we used a fluorescent dye, DAF-FM diacetate. DAF-FM fluorescence increased in response to high frequency stimulation but the increase was greater in the NMJs of SOD^{G93A} mice than in the WT mice (Fig. 5A). In SOD^{G93A} mice, the fluorescence increased by 19 ± 2% (n = 12 animals, $P < 0.01$) versus 5.2 ± 1.1% in the NMJs of WT mice (n = 10 animals, $P < 0.05$). Pre-incubation of the muscles from SOD^{G93A} mice with 24S-HC itself did not affect a DAF-FM fluorescence when compared to non-treated samples (Suppl. 3), but it completely abolished the enhancement of the DAF-FM fluorescence during high-frequency activity (n = 11 animals). In WT mice, 24S-HC also significantly suppressed the increase in DAF-FM fluorescence at 20 Hz stimulation (n = 12 animals). These data indicate that 24S-HC has a similar effect on NO production at the NMJs of SOD^{G93A} and WT mice.

To test the influence of 24S-HC-mediated suppression of NO production on synaptic vesicle exocytosis a NO synthase inhibitor, L-

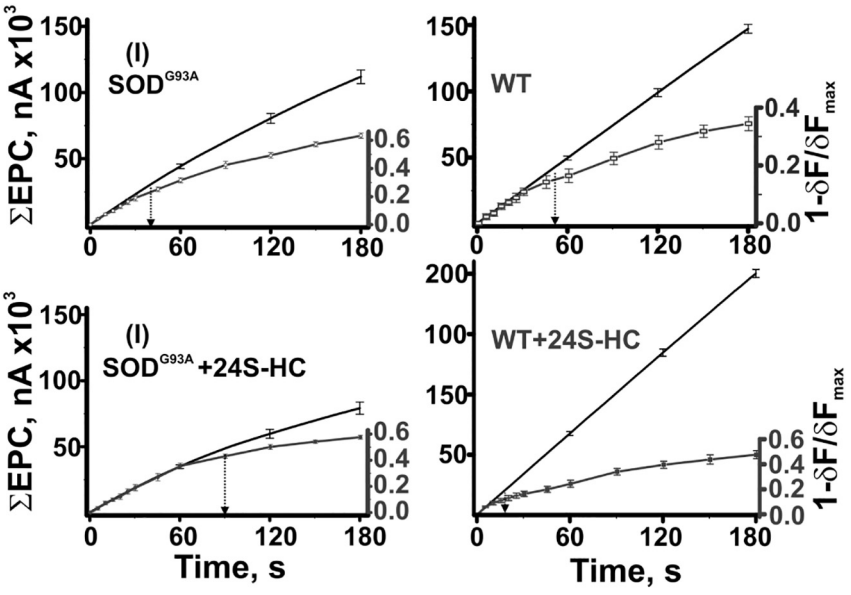

Fig. 4. Estimation of synaptic vesicle recycling time at 20 Hz stimulation. The inverted FM1-43 loss curve (gray lines; from Fig. 3B) are scaled to fit the initial part of the corresponding cumulative EPC amplitude curve (black lines; from Fig. 2B). The curves superimpose well at early times, but diverge at about 60 s in 24S-HC non-treated muscles or markedly greater and < 60 s in 24S-HC-treated NMJs of SOD^{G93A} and WT mice, receptively. This deviation (marked by arrow) results from synaptic vesicle reuse during prolonged high-frequency activity and indicates the average recycling time. For this comparison, the curves with fast FM1-43 unloading profiles (group I) were chosen because the recording of EPCs were performed only in the NMJs of SOD^{G93A} mice characterized by relatively high quantal content.

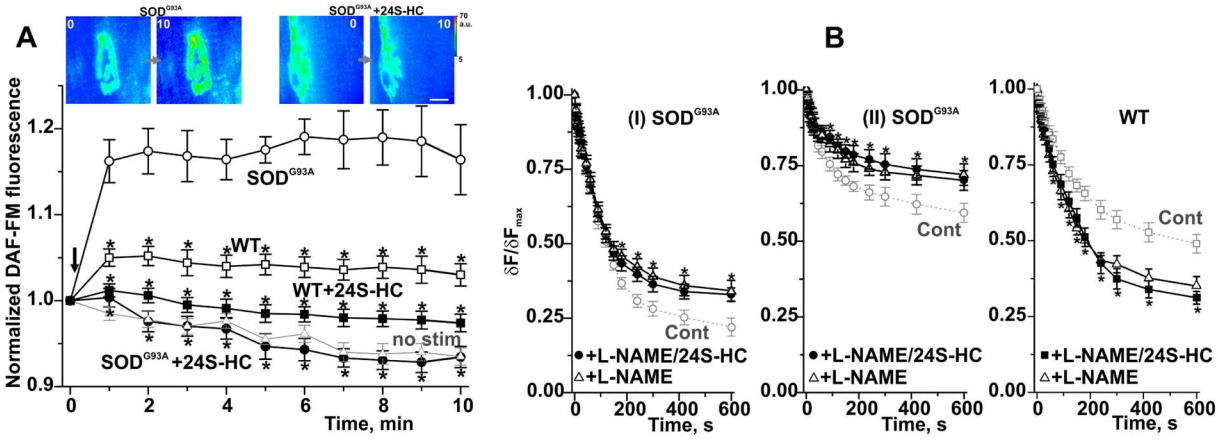

Fig. 5. Involvement of NO in 24S-HC-mediated modulation of synaptic vesicle exocytosis. A – time course of DAF-FM fluorescence during 20 Hz stimulation of NMJs. The onset of 20 Hz stimulation is marked by an arrow. A- at rest (without stimulation), DAF-FM fluorescence slowly decreased with time (a photobleaching curve; "no stim", n = 10 animals). High-frequency stimulation led to a slight or moderate increase in DAF-FM fluorescence in the NMJs of WT and SOD^{G93A} mice, respectively. 24S-HC pretreatment markedly inhibited the enhancement of the DAF-FM fluorescence in the NMJs of both WT and SOD^{G93A} mice. Top, pseudocolor images captured at 0 and 10 min of the stimulus train. The corresponding intensity scale is provided to the right (a.u.). Scale bar – 10 μm. Y-axis, shows normalized fluorescence intensity, with the initial fluorescence immediately prior to the stimulation taken as 1.0. Asterisks display significant differences ($P < 0.05$) from corresponding values in 24S-HC untreated NMJs of SOD^{G93A} mice. B – Influence of NO synthase inhibition with L-NAME on FM1-43 unloading kinetics in 24S-HC-treated and untreated NMJs. Like 24S-HC, L-NAME alone suppressed or accelerated the rate of FM1-43 unloading in SOD^{G93A} and WT mice, respectively (compare with Fig. 3B). Co-treatment with L-NAME and 24S-HC had no significant cumulative effect, indicating a similarity in the pathway of their action both in SOD^{G93A} and WT mice. This also suggests that the NO synthesis inhibitor modifies vesicle exocytosis in opposite ways in SOD^{G93A} and WT mice. (I) SOD^{G93A} and (II) SOD^{G93A}– graphs showing results obtained from NMJs with fast and slow FM1-43 destaining profiles, respectively.

NAME, was applied (Fig. 5B). In SOD^{G93A} mice, inhibition of NO synthesis decreased the rate of FM1-43 dye unloading beginning after 1–2 min of 20 Hz stimulation in the NMJs characterized by both high (group I) and low (group II) initial fluorescence (n = 6/6 animals). Under the conditions of NO synthase inhibition, 24S-HC had no additional influence on the kinetics of FM1-43 unloading in either group (n = 6/6 animals). In WT mice (Fig. 5B), L-NAME itself accelerated the rate of FM1-43 loss during high frequency stimulation (n = 10 animals) and 24S-HC had no additional effect on the kinetics of dye unloading in the L-NAME-treated muscles (n = 11 animals). These data suggest that the mechanism by which 24S-HC modulates synaptic vesicle exocytosis during high-frequency activity is related to a decrease in NO synthase activity in the NMJs of both SOD^{G93A} and WT mice: at the same time, inhibition of NO synthesis has the opposite effects on the evoked exocytosis in SOD^{G93A} versus WT mice.

3.4. Does 24S-HC modify NO production through a lipid raft-dependent pathway?

Previously, we have shown that in WT mice 24S-HC acts on NO production in a manner similar to the caveolin-1 scaffolding domain peptide (Kasimov et al., 2017), which usually mimics the effects of raft-resident proteins caveolins (Marchand et al., 2002; Gratton et al., 2003). The lipid raft integrity may be required for caveolin-dependent inhibition of NO synthase (García-Cardeña et al., 1997; El-Yazbi et al., 2008; Hutchinson et al., 2009). Additionally, cholesterol-like molecules can affect lipid-ordering in different cell types (Filomenko et al., 2015; Kasimov et al., 2015, 2016; Gambert et al., 2017). Consequently, one of the mechanisms for 24S-HC-dependent inhibition of the NO synthase activity may be linked with lipid raft integrity. To test this proposal, the membranes were stained with the lipid raft marker, CTxB. Additional labeling with Btx was used to identify the NMJ region (Fig. 6A). In SOD^{G93A} mice, the number of NMJs having high and low CTxB fluorescence was increased compared to that in WT mice, while the average intensity of CTxB fluorescence did not differ significantly between SOD^{G93A} (n = 6 animals) and WT (n = 6 animals) mice. Application of 24S-HC increased the mean fluorescence of CTxB (but not in extra-junctional regions; Suppl. 4) by 22.5 ± 4.3% ($P < 0.05$; n = 7 animals) and 23.5 ± 2.1% ($P < 0.05$; n = 6 animals) at the NMJs of SOD^{G93A} and WT mice, respectively (Fig. 6A, B). Note that the exposure to 24S-HC did not change the Btx fluorescence (Suppl. 4). For lipid raft manipulations, we used MβCD (at low concentration 0.1 mM) and exogenous SMase (0.1 u/ml) which are able to disturb the lipid rafts due to cholesterol redistribution and sphingomyelin hydrolysis. Indeed, treatment with either MβCD or SMase reduced the CTxB fluorescence by 14.8 ± 5.3% ($P < 0.05$; n = 5 animals) or 22.7 ± 4.8% ($P < 0.05$; n = 5 animals) in NMJs of WT mice, respectively. Both MβCD (n = 5 animals) and SMase (n = 5 animals) completely suppressed the 24S-HC-induced enhancement of CTxB staining in WT mice (Fig. 6B). These data suggest that 24S-HC could increase lipid raft stability in the synaptic region. This effect is prevented by MβCD or SMase.

Further, the idea that 24S-HC may suppress NO production by increasing lipid-raft integrity has received support from the observation that lipid-raft disrupting agents (MβCD or SMase) prevented the 24S-HC-mediated suppression of NO synthesis during high-frequency stimulation (n = 6/6 animals), while treatment with MβCD or SMase alone had no significant influence on the dynamics of DAF-FM fluorescence at 20 Hz activity (n = 5/5 animals) in the NMJs of SOD^{G93A} mice (Fig. 6C). It should be noted that 0.1 mM MβCD did not decrease the fluorescence of filipin III (a cholesterol binding antibiotic) in the NMJs of mice diaphragm (Kravtsova et al., 2015). This suggests that 0.1 mM MβCD disrupts lipid rafts by redistributing membrane cholesterol rather than by sequestering cholesterol from the plasma membrane (Zidovetzki and Levitan, 2007).

4. Discussion

4.1. 24S-HC and synaptic vesicle cycle at the NMJs of SOD^{G93A} mice

Despite a marked effect on spontaneous exocytosis, evoked neurotransmitter release at low frequency stimulation was not affected by 24S-HC at NMJs of SOD^{G93A} mice. By contrast, in WT mice 24S-HC slightly increased acetylcholine release in response to a single stimulus, but did not modify spontaneous release. This is consistent with the possibility that distinct mechanisms regulate spontaneous and evoked transmitter release (Kaeser and Regehr, 2017). For instance, pharmacological manipulations of the membrane cholesterol level and

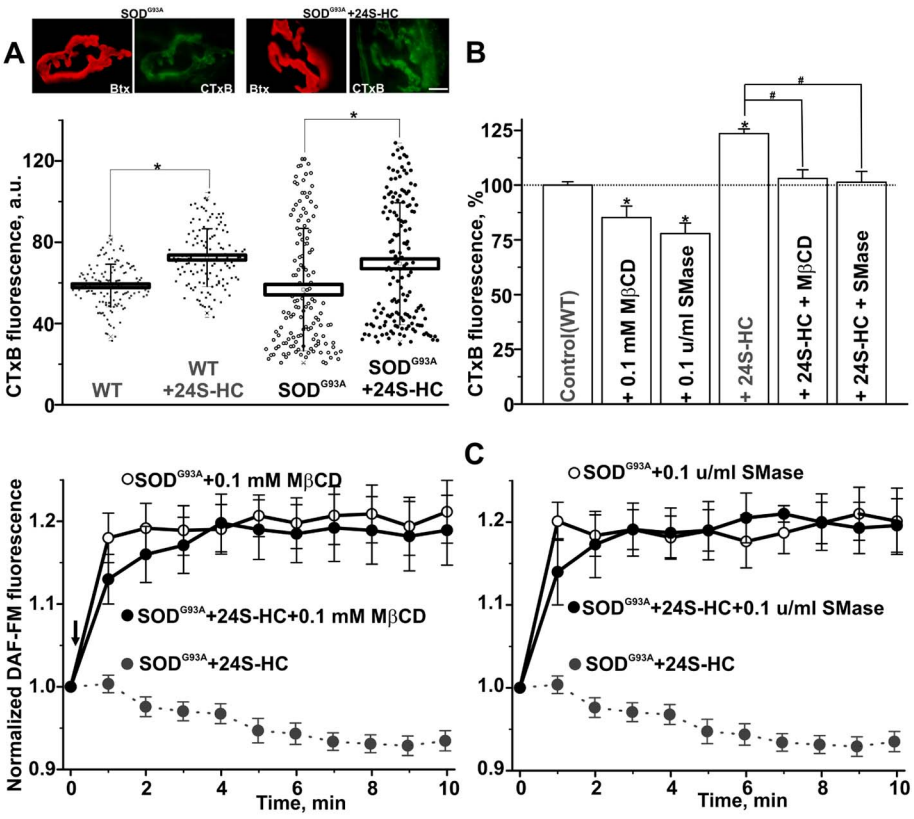

Fig. 6. Role of lipid rafts in the effect of 24S-HC on NO production at NMJs. A – Lipid raft labeling with CTxB. The muscles from WT and SOD^{G93A} mice were stained with rhodamine-conjugated αBtx (red channel) and Alexa488-conjugated CTxB (green channel). Top, fluorescent images of 24S-HC-treated and non-treated NMJs of SOD^{G93A} mice. Bottom, - the box plots indicate the changes in CTxB fluorescence; all measurements from 6 to 7 different animals for each plot (points), mean value (square), standard error (box range) and standard deviation (whisker) are shown. Only for this graph, the means were calculated as arithmetic averages of all measurements. The increase in CTxB fluorescence after pre-exposure to 24S-HC suggests an enhanced lipid raft stability in both WT and SOD^{G93A} mice. Y-axis – fluorescence in a.u. B – Lipid manipulations prevented the effects of 24S-HC on CTxB staining of NMJs from WT mice. Exposure to MβCD or SMase decreased the CTxB-labeling of NMJs and prevented the 24S-HC-mediated increase in CTxB fluorescence. C – Change in DAF-FM fluorescence during 20 Hz simulation in NMJs of SOD^{G93A} mice. Lipid-raft disrupting agents (MβCD and SMase) abolished the depressant action of 24S-HC on the DAF-FM fluorescence, while pretreatment with MβCD (or SMase) alone had no significant influence on the increase in DAF-FM fluorescence at the NMJs of the SOD^{G93A} mice. Other details are as in Fig. 5. (For interpretation of the references to colour in this figure legend, the reader is referred to the web version of this article.)

treatment with oxysterol or 5α-cholestan-3-one, modulate spontaneous and evoked neurotransmitter release in different ways (Zamir and Charlton, 2006; Teixeira et al., 2012; Rodrigues et al., 2013; Petrov et al., 2014; Kasimov et al., 2016). The observed changes in the effects of 24S-HC on spontaneous and evoked transmitter release in the ALS model mice may be related to alterations of the signaling pathway(s) that control the balance between spontaneous and evoked transmitter release during the progression of ALS.

Evoked neurotransmitter release in response to low frequency activity mainly depends on the probability of exocytosis and the size of ready releasable pool (Kaeser and Regehr, 2017). However, during moderate and strong activity, the amount of quantal release is also determined by recruitment of synaptic vesicles to the active zone and their recycling (Rizzoli and Betz, 2005; Slater, 2015). The depression of both neurotransmitter release and FM1-43 dye loss during high-frequency stimulation was greater after pretreatment with 24S-HC in SOD^{G93A} mice. Eventually, this resulted in reduced neurotransmitter release (summed EPCs) after 3 min of high-frequency activity. This suggests that in SOD^{G93A} mice, 24S-HC suppresses synaptic transmission by decreasing the recruitment of neurotransmitter-filled synaptic vesicle for exocytosis upon intense activity. The absence of changes in MEPC amplitudes immediately prior to and at the end of high frequency stimulation argues against the possibility that the deficit in synaptic vesicle refilling contributes to the EPC depression. Additionally, 24S-HC interfered with recovery of neurotransmitter release after high-frequency stimulation, probably due to a reduced rate of delivery of synaptic vesicles to the active zone or to a defect in their fusion-competence. The marked effect of 24S-HC on transmitter release in response to intense activity, but not to single stimulus, suggests a preferential action on synaptic vesicle mobilization and endocytosis (Rizzoli and Betz, 2005). For instance, up- or downregulation of cGMP signaling significantly changes synaptic vesicle cycling and the rate of synaptic depression during high-frequency stimulation without affecting neurotransmitter release at low-frequency stimulation in the frog NMJs (Petrov et al., 2008).

Despite on the rapid attenuation of neurotransmitter release, 24S-HC did not markedly modify the rate of FM1-43 loss during the first 1–2 min of high-frequency stimulation in SOD^{G93A} mice. Under these conditions, dye unloading only began to slow down after 2–3 min of stimulation. Comparison of the rates of neurotransmitter release and of FM-dye loss indicates an increase in the mean time required for synaptic vesicle recycling in 24S-HC treated NMJs. Thus, the discrepancy between the rates of neurotransmitter release and FM-dye exocytosis may arise from 24S-HC mediated reduction of the rate of synaptic vesicle reuse during high frequency activity. This might have a protective effect, since enhanced acetylcholine release due to an overexpression of VAchT in the motor neurons accelerates degeneration of NMJs in the SOD^{G93A} mouse (Sugita et al., 2016). Motor neurons with fast-fatigable characteristics are lost first in ALS, but before any structural alteration of the NMJs, their quantal contents are already higher than in WT mice (Tremblay et al., 2017). The decreased rate of spontaneous release may also have a beneficial effect, inhibiting the progression of ALS (Uchitel et al., 1992). On the other hand, the enhanced synaptic depression and disrupted post-tetanic potentiation might aggravate the failure of neuromuscular transmission in ALS mice.

It is likely that 24S-HC-mediated suppression of synaptic vesicle cycling reveals a defect in either the mechanism of endocytosis or in sorting of the synaptic vesicle proteins in ALS mice. Using a Drosophila model of ALS, it was shown that TDP-43 toxicity results in part from impaired activity of the synaptic CSP/Hsc70 chaperone complex impacting dynamin function in endocytosis (Coyne et al., 2017). Synaptic vesicle endocytosis and membrane trafficking were impaired in the NMJs of transgenic mice expressing ubiquitinated synaptobrevin 2 and exerting ALS-like phenotype (Liu et al., 2015).

During the progression of ALS, neuromuscular transmission is affected in a time- and muscle-specific manner (Rocha et al., 2013; Nascimento et al., 2015; Tremblay et al., 2017). Although respiratory failure is generally the cause of death in ALS, the results concerning the influence of this disorder on neurotransmission in the diaphragm are contradictory. Immunoglobulins from ALS patient may increase

spontaneous transmitter release in mouse phrenic nerve-diaphragm preparations (Uchitel et al., 1992). By contrast, SOD1^{G93A} mice at an early symptomatic stage display a reduced frequency of spontaneous release in the diaphragm muscle without changes in transmitter release evoked by single nerve stimulus (Naumenko et al., 2011). Another study showed enhanced evoked transmitter release at 0.5 Hz in the pre-symptomatic phase of SOD1^{G93A} mice and a separation of NMJs in the symptomatic phase into two groups characterized by either reduced amplitude of both miniature and evoked postsynaptic responses or with no difference from WT nor pre-symptomatic SOD1^{G93A} mice (Rocha et al., 2013).

Here, we found a decrease in total transmitter release during high-frequency in SOD1^{G93A} mice without a change in the mean synaptic vesicle recycling time or MEPC amplitude. In addition, we revealed two types of NMJs in the diaphragms of SOD1^{G93A} mice, characterized by low and high ability to take up and release FM1-43 dye in response to intense activity. This is consistent with electron microscopic data showing a reduction of the synaptic vesicle pool in approximately 40% of the presynaptic terminals in the diaphragms of SOD1^{G93A} mice at the time of symptom onset (Cappello et al., 2012). Labeling with CTxB also suggests that there are more NMJs with lower and higher “amounts” of lipid rafts in SOD1^{G93A} mice than in WT mice. The rafts can contain many proteins involved in the exo-endocytic cycle (Gil et al., 2006). Evidence about the presence of different populations of NMJs may reflect the simultaneous occurrence of two processes: one, a progressive presynaptic dysfunction that precedes the detachment of nerve terminals, the other, a compensation for the loss of innervation, involving enhanced synaptic transmission in the remaining functionally active NMJs (Gordon et al., 2010; Rocha et al., 2013; Nijssen et al., 2017). Alternatively, NMJs innervating different fiber types (slow, fast fatigue-resistant and fast-fatigable) might experience the opposite synaptic alterations in ALS mice (Tremblay et al., 2017). The diaphragm is a mixed muscle consisting of both fast and slow twitch fibers, and the fast muscle fibers and corresponding NMJs are preferentially affected by ALS (Atkin et al., 2005; Gordon et al., 2010).

Altogether, the increased depression of transmitter release, the unchanged time of vesicle recycling, and the presence of NMJs able to uptake and release more FM1-43 dye in response to high frequency stimulation may reflect (1) a decrease in the population of synaptic vesicles reused during activity (the “recycling” pool) and (2) a compensation for this by recruitment of vesicles from the reserve pool in NMJs of SOD1^{G93A}.

4.2. Implication of NO and lipid rafts in the action of 24S-HC

In WT mice, 24S-HC has the opposite effect on neuromuscular transmission from those in the SOD1^{G93A} mice. In particular, 24S-HC increases the rate of synaptic vesicle cycling due to an attenuation of NO signaling, which normally suppresses synaptic vesicle exocytosis in WT mice NMJs (Kasimov et al., 2017). Surprisingly, in the NMJs of SOD1^{G93A} mice, 24S-HC also significantly attenuated NO production during high-frequency activity. It is likely that NO-mediated modulation of synaptic vesicle exocytosis is changed in SOD1^{G93A} mice. In support of this, by acting in a manner similar to that of 24S-HC in SOD1^{G93A} mice, inhibition of NO synthesis by L-NAME suppresses FM1-43 unloading. L-NAME had the opposite effect at the NMJs of WT mice. Further, L-NAME completely masked the effect of 24S-HC in both SOD1^{G93A} and WT mice. These data indicate that the common pathway by which 24S-HC modifies exocytosis during intense activity involves a suppression of NO synthase activity in the NMJs of both WT and SOD1^{G93A} mice. However, decreased NO synthesis promotes or attenuates the synaptic vesicle exocytosis during intense activity in WT or SOD1^{G93A} mice, respectively. It is unclear why the effect of NO signaling on synaptic vesicle exocytosis is reversed in the diaphragm of SOD^{G93A} mice. One possibility is that different signaling pathways downstream of NO might have opposite effects on transmitter release and the rate of recycling at NMJs (Thomas and Robitaille, 2001; Petrov et al., 2008; Zhu et al., 2013). Possibly changes in these signaling pathways occur during the ALS progression.

Here, we found that activity-induced NO production at the NMJs was significantly upregulated in the SOD1^{G93A} mice. Previously, increased NOS expression at synaptic sites on anterior horn neurons was shown in patients with sporadic ALS (Sasaki et al., 2001). Embryonic motor neurons from mutant SOD mouse models, but not from WT mice, can be triggered to die by exposure to NO, leading to activation of a motor neuron-specific signaling pathway (Duplan et al., 2010). Chronic treatment with an antagonist of NO synthase reduced inhibitory synapse loss on motor neurons in SOD^{G93A} mice (Sunico et al., 2011). Delivery of IGF-1 to the central nervous system reduced ALS pathology partially by attenuating glial-cell-mediated release TNF-α and NO (Dodge et al., 2008). In this scenario, 24S-HC-mediated suppression of NO overproduction at the NMJs may have a potentially protective effect in the ALS model.

Previously, we showed that 24S-HC modulates NO production that is selectively inhibited by cavtratin, a caveolin-1 scaffolding domain peptide (Kasimov et al., 2017). This peptide, acting in the same manner as caveolin scaffolding domain, interacts with different signaling molecules (including NO synthase) and restricts their activity (García-Cardeña et al., 1997; Michel et al., 1997; Gratton et al., 2003). Caveolins are normally concentrated within the lipid raft fraction and NMJs are enriched with caveolins that interact with synaptic-specific proteins (Marchand et al., 2002; Hezel et al., 2010; Heiny et al., 2010). Acute lipid raft disturbance due to cholesterol depletion might upregulate NO synthase activity and eliminate caveolin-3-endothelial NO synthase binding in cardiomyocytes (Ostrom et al., 2004; El-Yazbi et al., 2008; Hutchinson et al., 2009; Odnoshivkina et al., 2017), while hypercholesterolemia may decrease NO production by promoting the interaction of caveolin and endothelial NO synthase in endothelial cells (Feron et al., 1999). We have also previously shown that cholesterol-like molecules may affect lipid raft integrity at the NMJ (Kasimov et al., 2015, 2016). In addition, a recent study indicates that 24S-HC alters membrane dynamics involving lipid rafts in Muller Glial Cells (Gambert et al., 2017).

Here, we observed that 24S-HC increases the staining of NMJ membranes with CTxB (a lipid raft marker), indicating an increase in membrane ordering. Moreover, treatment with raft-disrupting agents (MβCD or SMase) markedly suppressed the effect of 24S-HC on both lipid raft integrity and activity-induced NO production. It is likely that 24S-HC attenuates NO production by increasing lipid raft stability at the NMJs. Given that the disturbance of cholesterol-rich microdomans at the NMJ might occur as a result of muscle disuse, and might also affect synaptic transmission (Marchand et al., 2002; Gil et al., 2006; Assaife-Lopes et al., 2014; Petrov et al., 2011, 2017b), the potential membrane ordering effect of 24S-HC might protect NMJs from functional deficits and detachment. Disruption of lipid rafts is known to have inhibitory effects especially on signaling through the receptors of trophic factors belonging to the tyrosine-kinase family (Assaife-Lopes et al., 2014; Sural-Fehr and Bongarzone, 2016).

4.3. Possible pathophysiological significance

The pathophysiological relevance of 24S-HC-mediated effects on the NMJs is unknown. The plasma level of the 24S-HC is determined by the balance between its production in the brain and clearance by the liver. It is likely that biphasic changes in 24S-HC synthesis, involving elevation followed by decline, occur during progression of ALS (Leoni and Caccia, 2013; Wuolikainen et al., 2014; Abdel-Khalik et al., 2017). One possibility is that disease-associated changes in 24S-HC plasma level modulate synaptic communication in the diaphragm. In principle, an increased level of 24S-HC may have a protective effect in the NMJs of ALS model by preventing lipid raft disturbance and excess release of both acetylcholine and NO. 24S-HC plays a neuroprotective role in

glaucoma (Ishikawa et al., 2016) and it delays the decrease in choline acetyltransferase-positive neurons in organotypic brain slices of the basal nucleus (Ullrich et al., 2010). According to these premises, pharmacological activation of CYP46A1 with efavirenz (Mast et al., 2017) may be potentially useful for ALS therapy. However, 24S-HC may exert toxic effects under some experimental conditions (Sun et al., 2017). Recently, it was shown that the serum level of 25-HC was significantly higher in ALS patients than in controls, and its level was associated with disease severity (Kim et al., 2017). One of the main sources of 25-HC are macrophages and mast cells that could interact with degenerating NMJs, thereby promoting distal axonopathy in the SOD^{G93A} rat (Trias et al., 2017). Given that 24S-HC and 25-HC might exert opposite influences on cellular events, including neuronal survival (Ullrich et al., 2010; Sun et al., 2017), there is the possibility of a competitive relation between 24S-HC and 25-HC in the progression of ALS.

Our experiments were carried out near room temperature, which is far from the physiological conditions. Synaptic vesicle retrieval, NO synthesis and lipid raft behavior are temperature-dependent. In particular, the rate of synaptic depression at high-frequency stimulation was greater at 20 °C than it was at physiological temperature in the diaphragm of rat (Moyer and van Lunteren, 2001). This is consistent with the proposal that the rate of synaptic vesicle exo-endocytosis may be higher at physiological temperature (Micheva and Smith, 2005). An increase in temperature can enhance the catalytic activity of NO synthases (Venturini et al., 1999) and may influence the stability of synaptic lipid rafts (Gil et al., 2006). Thus, temperature may affect on magnitude of the 24S-HC effects. Additionally, the results of this research are subject to the limitations of pharmacological manipulations. Thus, further studies at physiological temperature, using molecular and genetics approaches, are required to identify the precise mechanism by which 24S-HC modulates the neuromuscular transmission.

Supplementary data to this article can be found online at https://doi.org/10.1016/j.mcn.2018.03.006.

Acknowledgments

We thank Professor Clarke Slater (Newcastle University) for helpful comments on the manuscript. This study was funded by the grants from RFBR# 17-04-00046 and RSF# 14-15-00847 and the program for support of bioresource collections of FASO.

Author contributions

K.A.M, M.R.K., A.R.G. and G.F.Z. performed all experiments, data collection and analysis. A.M.P. interpreted results of experiments, designed and wrote the manuscript. All the authors read and approved the final version of manuscript.

Conflict of interest statement

There are no competing interests.

References

Abdel-Khalik, J., Yutuc, E., Crick, P.J., Gustafsson, J.Å., Warner, M., Roman, G., Talbot, K., Gray, E., Griffiths, W.J., Turner, M.R., Wang, Y., 2017. Defective cholesterol metabolism in amyotrophic lateral sclerosis. J. Lipid Res. 58 (1), 267–278. http://dx.doi.org/10.1194/jlr.P071639.

Arbour, D., Tremblay, E., Martineau, É., Julien, J.P., Robitaille, R., 2015. Early and persistent abnormal decoding by glial cells at the neuromuscular junction in an ALS model. J. Neurosci. 35 (2), 688–706. http://dx.doi.org/10.1523/JNEUROSCI.1379-14.2015.

Assaife-Lopes, N., Sousa, V.C., Pereira, D.B., Ribeiro, J.A., Sebastião, A.M., 2014. Regulation of TrkB receptor translocation to lipid rafts by adenosine A(2A) receptors and its functional implications for BDNF-induced regulation of synaptic plasticity. Purinergic Signal 10 (2), 251–267. http://dx.doi.org/10.1007/s11302-013-9389-9.

Atkin, J.D., Scott, R.L., West, J.M., Lopes, E., Quah, A.K., Cheema, S.S., 2005. Properties of slow- and fast-twitch muscle fibres in a mouse model of amyotrophic lateral sclerosis. Neuromuscul. Disord. 15, 377–388. http://dx.doi.org/10.1016/j.nmd.2005.02.005.

Babiker, A., Diczfalusy, U., 1998. Transport of side-chain oxidized oxysterols in the human circulation. Biochim. Biophys. Acta 1392 (2–3), 333–339.

Cappello, V., Vezzoli, E., Righi, M., Fossati, M., Mariotti, R., Crespi, A., Patruno, M., Bentivoglio, M., Pietrini, G., Francolini, M., 2012. Analysis of neuromuscular junctions and effects of anabolic steroid administration in the SOD1G93A mouse model of ALS. Mol. Cell. Neurosci. 51 (1–2), 12–21. http://dx.doi.org/10.1016/j.mcn.2012.07.003.

Coyne, A.N., Lorenzini, I., Chou, C.C., Torvund, M., Rogers, R.S., Starr, A., Zaepfel, B.L., Levy, J., Johannesmeyer, J., Schwartz, J.C., Nishimune, H., Zinsmaier, K., Rossoll, W., Sattler, R., Zarnescu, D.C., 2017. Post-transcriptional inhibition of Hsc70-4/HSPA8 expression leads to synaptic vesicle cycling defects in multiple models of ALS. Cell Rep. 21 (1), 110–125. http://dx.doi.org/10.1016/j.celrep.2017.09.028.

Crick, P.J., Beckers, L., Baes, M., Van Veldhoven, P.P., Wang, Y., Griffiths, W.J., 2015. The oxysterol and cholestenoic acid profile of mouse cerebrospinal fluid. Steroids 99 (Pt B), 172–177. http://dx.doi.org/10.1016/j.steroids.2015.02.021.

Dodge, J.C., Haidet, A.M., Yang, W., Passini, M.A., Hester, M., Clarke, J., Roskelley, E.M., Treleaven, C.M., Rizo, L., Martin, H., Kim, S.H., Kaspar, R., Taksir, T.V., Griffiths, D.A., Cheng, S.H., Shihabuddin, L.S., Kaspar, B.K., 2008. Delivery of AAV-IGF-1 to the CNS extends survival in ALS mice through modification of aberrant glial cell activity. Mol. Ther. 16 (6), 1056–1064. http://dx.doi.org/10.1038/mt.2008.60.

Dumolt, J.H., Radhakrishnan, S.K., Moghadasian, M.H., Le, K., Patel, M.S., Browne, R.W., Rideout, T.C., 2017. Maternal hypercholesterolemia enhances oxysterol concentration in mothers and newly weaned offspring but is attenuated by maternal phytosterol supplementation. J. Nutr. Biochem. 52, 10–17. http://dx.doi.org/10.1016/j.jnutbio.2017.09.013.

Duplan, L., Bernard, N., Casseron, W., Dudley, K., Thouvenot, E., Honnorat, J., Rogemond, V., De Bovis, B., Aebischer, P., Marin, P., Raoul, C., Henderson, C.E., Pettmann, B., 2010. Collapsin response mediator protein 4a (CRMP4a) is upregulated in motoneurons of mutant SOD1 mice and can trigger motoneuron axonal degeneration and cell death. J. Neurosci. 30 (2), 785–796. http://dx.doi.org/10.1523/JNEUROSCI.5411-09.2010.

Dupuis, L., Corcia, M.D., Corcia, P., Fergani, A., Gonzalez de Aguila, J.L., Bonnefont-Rousselot, D., Bittar, R., Seilhean, D., Hauw, J.J., Lacomblez, L., Loeffler, J.P., Meininger, V., 2008. Dyslipidemia is a protective factor in amyotrophic lateral sclerosis. Neurology 70, 1004–1009. http://dx.doi.org/10.1212/01.wnl.0000285080.70324.27.

El-Yazbi, A.F., Cho, W.J., Cena, J., Schulz, R., Daniel, E.E., 2008. Smooth muscle NOS, colocalized with caveolin-1, modulates contraction in mouse small intestine. J. Cell. Mol. Med. 12 (4), 1404–1415. http://dx.doi.org/10.1111/j.1582-4934.2008.00335.x.

Feron, O., Dessy, C., Moniotte, S., Desager, J.P., Balligand, J.L., 1999. Hypercholesterolemia decreases nitric oxide production by promoting the interaction of caveolin and endothelial nitric oxide synthase. J. Clin. Invest. 103 (6), 897–905. http://dx.doi.org/10.1172/JCI4829.

Filomenko, R., Fourgeux, C., Bretillon, L., Gambert-Nicot, S., 2015. Oxysterols: influence on plasma membrane rafts microdomains and development of ocular diseases. Steroids 99 (Pt B), 259–265. http://dx.doi.org/10.1016/j.steroids.2015.02.004.

Fischer, L.R., Culver, D.G., Tennant, P., Davis, A.A., Wang, M., Castellano-Sanchez, A., Khan, J., Polak, M.A., Glass, J.D., 2004. Amyotrophic lateral sclerosis is a distal axonopathy: evidence in mice and man. Exp. Neurol. 185, 232–240. http://dx.doi.org/10.1016/j.expneurol.2003.10.004.

Gambert, S., Gabrielle, P.H., Masson, E., Leger-Charnay, E., Ferrerro, A., Vannier, A., Gendrault, C., Lachot, M., Creuzot-Garcher, C., Bron, A., Gregoire, S., Leclere, L., Martine, L., Lucchi, G., Truntzer, C., Pecqueur, D., Bretillon, L., 2017. Cholesterol metabolism and glaucoma: modulation of Muller cell membrane organization by 24S-hydroxycholesterol. Chem. Phys. Lipids 207 (Pt B), 179–191. http://dx.doi.org/10.1016/j.chemphyslip.2017.05.007.

García-Cardeña, G., Martasek, P., Masters, B.S., Skidd, P.M., Couet, J., Li, S., Lisanti, M.P., Sessa, W.C., 1997. Dissecting the interaction between nitric oxide synthase (NOS) and caveolin. Functional significance of the nos caveolin binding domain in vivo. J. Biol. Chem. 272 (41), 25437–25440.

Gil, C., Cubí, R., Blasi, J., Aguilera, J., 2006. Synaptic proteins associate with a sub-set of lipid rafts when isolated from nerve endings at physiological temperature. Biochem. Biophys. Res. Commun. 348 (4), 1334–1342.

Glavinović, M.I., 1979. Voltage clamping of unparalysed cut rat diaphragm for study of transmitter release. J. Physiol. 290 (2), 467–480.

Gordon, T., Tyreman, N., Li, S., Putman, C.T., Hegedus, J., 2010. Functional over-load saves motor units in the SOD1-G93A transgenic mouse model of amyotrophic lateral sclerosis. Neurobiol. Dis. 37 (2), 412–422. http://dx.doi.org/10.1016/j.nbd.2009.10.021.

Gratton, J.P., Lin, M.I., Yu, J., Weiss, E.D., Jiang, Z.L., Fairchild, T.A., Iwakiri, Y., Groszmann, R., Claffey, K.P., Cheng, Y.C., Sessa, W.C., 2003. Selective inhibition of tumor microvascular permeability by cavtratin blocks tumor progression in mice. Cancer Cell 4 (1), 31–39.

Gurney, M.E., Pu, H., Chiu, A.Y., Dal Canto, M.C., Polchow, C.Y., Alexander, D.D., Caliendo, J., Hentati, A., Kwon, Y.W., Deng, H.X., et al., 1994. Motor neuron degeneration in mice that express a human Cu, Zn superoxide dismutase mutation. Science 264 (5166), 1772–1775. http://dx.doi.org/10.1126/science.8209258.

Heiny, J.A., Kravtsova, V.V., Mandel, F., Radzyukevich, T.L., Benziane, B., Prokofiev, A.V., Pedersen, S.E., Chibalin, A.V., Krivoi, I.I., 2010. The nicotinic acetylcholine receptor and the Na,K-ATPase alpha2 isoform interact to regulate membrane electrogenesis in skeletal muscle. J. Biol. Chem. 285 (37), 28614–28626. http://dx.doi.org/10.1074/jbc.M110.150961.

Hezel, M., de Groat, W.C., Galbiati, F., 2010. Caveolin-3 promotes nicotinic acetylcholine

receptor clustering and regulates neuromuscular junction activity. Mol. Biol. Cell 21 (2), 302–310. http://dx.doi.org/10.1091/mbc.E09-05-0381.
Hutchinson, T.E., Kuchibhotla, S., Block, E.R., Patel, J.M., 2009. Peptide-stimulation enhances compartmentalization and the catalytic activity of lung endothelial NOS. Cell. Physiol. Biochem. 24 (5–6), 471–482. http://dx.doi.org/10.1159/000257487.
Ishikawa, M., Yoshitomi, T., Zorumski, C.F., Izumi, Y., 2016. 24(S)-hydroxycholesterol protects the ex vivo rat retina from injury by elevated hydrostatic pressure. Sci. Rep. 6, 33886. http://dx.doi.org/10.1038/srep33886.
Kaeser, P.S., Regehr, W.G., 2017. The readily releasable pool of synaptic vesicles. Curr. Opin. Neurobiol. 43, 63–70. http://dx.doi.org/10.1016/j.conb.2016.12.012.
Kasimov, M.R., Fatkhrakhmanova, M.R., Mukhutdinova, K.A., Petrov, A.M., 2017. 24S-hydroxycholesterol enhances synaptic vesicle cycling in the mouse neuromuscular junction: implication of glutamate NMDA receptors and nitric oxide. Neuropharmacology 117, 61–73. http://dx.doi.org/10.1016/j.neuropharm.2017.01.030.
Kasimov, M.R., Giniatullin, A.R., Zefirov, A.L., Petrov, A.M., 2015. Effects of 5α-cholestan-3-one on the synaptic vesicle cycle at the mouse neuromuscular junction. Biochim. Biophys. Acta 1851 (5), 674–685. http://dx.doi.org/10.1016/j.bbalip.2015.02.012.
Kasimov, M.R., Zakyrjanova, G.F., Giniatullin, A.R., Zefirov, A.L., Petrov, A.M., 2016. Similar oxysterols may lead to opposite effects on synaptic transmission: olesoxime versus 5α-cholestan-3-one at the frog neuromuscular junction. Biochim. Biophys. Acta 1861 (7), 606–616. http://dx.doi.org/10.1016/j.bbalip.2016.04.010.
Kim, S.M., Noh, M.Y., Kim, H., Cheon, S.Y., Lee, K.M., Lee, J., Cha, E., Park, K.S., Lee, K.W., Sung, J.J., Kim, S.H., 2017. 25-Hydroxycholesterol is involved in the pathogenesis of amyotrophic lateral sclerosis. Oncotarget 8 (7), 11855–11867. http://dx.doi.org/10.18632/oncotarget.14416.
Kravtsova, V.V., Petrov, A.M., Vasil'ev, A.N., Zefirov, A.L., Krivoi, I.I., 2015. Role of cholesterol in the maintenance of endplate electrogenesis in rat diaphragm. Bull. Exp. Biol. Med. 158 (3), 298–300. http://dx.doi.org/10.1007/s10517-015-2745-8.
La Marca, V., Maresca, B., Spagnuolo, M.S., Cigliano, L., Dal Piaz, F., Di Iorio, G., Abrescia, P., 2016. Lecithin-cholesterol acyltransferase in brain: does oxidative stress influence the 24-hydroxycholesterol esterification? Neurosci. Res. 105, 19–27. http://dx.doi.org/10.1016/j.neures.2015.09.008.
Leoni, V., Caccia, C., 2013. 24S-hydroxycholesterol in plasma: a marker of cholesterol turnover in neurodegenerative diseases. Biochimie 95 (3), 595–612. http://dx.doi.org/10.1016/j.biochi.2012.09.025.
Liu, Y., Li, H., Sugiura, Y., Han, W., Gallardo, G., Khvotchev, M., Zhang, Y., Kavalali, E.T., Südhof, T.C., Lin, W., 2015. Ubiquitin-synaptobrevin fusion protein causes degeneration of presynaptic motor terminals in mice. J. Neurosci. 35 (33), 11514–11531. http://dx.doi.org/10.1523/JNEUROSCI.5288-14.2015.
Lütjohann, D., Breuer, O., Ahlborg, G., Nennesmo, I., Sidén, A., Diczfalusy, U., Björkhem, I., 1996. Cholesterol homeostasis in human brain: evidence for an age-dependent flux of 24S-hydroxycholesterol from the brain into the circulation. Proc. Natl. Acad. Sci. U. S. A. 93 (18), 9799–9804.
Marchand, S., Devillers-Thiéry, A., Pons, S., Changeux, J.P., Cartaud, J., 2002. Rapsyn escorts the nicotinic acetylcholine receptor along the exocytic pathway via association with lipid rafts. J. Neurosci. 22 (20), 8891–8901.
Mast, N., Saadane, A., Valencia-Olvera, A., Constans, J., Maxfield, E., Arakawa, H., Li, Y., Landreth, G., Pikuleva, I.A., 2017. Cholesterol-metabolizing enzyme cytochrome P450 46A1 as a pharmacologic target for Alzheimer's disease. Neuropharmacology 123, 465–476. http://dx.doi.org/10.1016/j.neuropharm.2017.06.026.
Meng, L.J., Griffiths, W.J., Nazer, H., Yang, Y., Sjövall, J., 1997. High levels of (24S)-24-hydroxycholesterol 3-sulfate, 24-glucuronide in the serum and urine of children with severe cholestatic liver disease. J. Lipid Res. 38 (5), 926–934.
Michel, J.B., Feron, O., Sacks, D., Michel, T., 1997. Reciprocal regulation of endothelial nitric-oxide synthase by Ca2+-calmodulin and caveolin. J. Biol. Chem. 272 (25), 15583–15586.
Micheva, K.D., Smith, S.J., 2005. Strong effects of subphysiological temperature on the function and plasticity of mammalian presynaptic terminals. J. Neurosci. 25 (33), 7481–7488.
Moyer, M., van Lunteren, E., 2001. Effect of temperature on endplate potential rundown and recovery in rat diaphragm. J. Neurophysiol. 85 (5), 2070–2075.
Narai, H., Manabe, Y., Nagai, M., Nagano, I., Ohta, Y., Murakami, T., Takehisa, Y., Kamiya, T., Abe, K., 2009. Early detachment of neuromuscular junction proteins in ALS mice with SODG93A mutation. Neurol. Int. 1 (1), e16. http://dx.doi.org/10.4081/ni.2009.e16.
Nascimento, F., Sebastião, A.M., Ribeiro, J.A., 2015. Presymptomatic and symptomatic ALS SOD1(G93A) mice differ in adenosine A1 and A2A receptor-mediated tonic modulation of neuromuscular transmission. Purinergic Signal 11 (4), 471–480. http://dx.doi.org/10.1007/s11302-015-9465-4.
Naumenko, N., Pollari, E., Kurronen, A., Giniatullina, R., Shakirzyanova, A., Magga, J., Koistinaho, J., Giniatullin, R., 2011. Gender-specific mechanism of synaptic impairment and its prevention by GCSF in a mouse model of ALS. Front. Cell. Neurosci. 5, 26. http://dx.doi.org/10.3389/fncel.2011.00026.
Nijssen, J., Comley, L.H., Hedlund, E., 2017. Motor neuron vulnerability and resistance in amyotrophic lateral sclerosis. Acta Neuropathol. 133 (6), 863–885. http://dx.doi.org/10.1007/s00401-017-1708-8.
Odnoshivkina, Y.G., Sytchev, V.I., Petrov, A.M., 2017. Cholesterol regulates contractility and inotropic response to β2-adrenoceptor agonist in the mouse atria: involvement of Gi-protein-Akt-NO-pathway. J. Mol. Cell. Cardiol. 107, 27–40. http://dx.doi.org/10.1016/j.yjmcc.2016.05.001.
Ostrom, R.S., Bundey, R.A., Insel, P.A., 2004. Nitric oxide inhibition of adenylyl cyclase type 6 activity is dependent upon lipid rafts and caveolin signaling complexes. J. Biol. Chem. 279 (19), 19846–19853.
Petrov, A.M., Giniatullin, A.R., Sitdikova, G.F., Zefirov, A.L., 2008. The role of cGMP-dependent signaling pathway in synaptic vesicle cycle at the frog motor nerve terminals. J. Neurosci. 28 (49), 13216–13222. http://dx.doi.org/10.1523/JNEUROSCI.2947-08.2008.
Petrov, A.M., Kasimov, M.R., Zefirov, A.L., 2017a. Cholesterol in the pathogenesis of Alzheimer's, Parkinson's diseases and autism: link to synaptic dysfunction. Acta Nat. 9 (1), 26–37.
Petrov, A.M., Kravtsova, V.V., Matchkov, V.V., Vasiliev, A.N., Zefirov, A.L., Chibalin, A.V., Heiny, J.A., Krivoi, I.I., 2017b. Membrane lipid rafts are disturbed in the response of rat skeletal muscle to short-term disuse. Am. J. Phys. Cell Physiol. 312 (5), C627–C637. http://dx.doi.org/10.1152/ajpcell.00365.2016.
Petrov, A.M., Naumenko, N.V., Uzinskaya, K.V., Giniatullin, A.R., Urazaev, A.K., Zefirov, A.L., 2011. Increased non-quantal release of acetylcholine after inhibition of endocytosis by methyl-β-cyclodextrin: the role of vesicular acetylcholine transporter. Neuroscience 186, 1–12. http://dx.doi.org/10.1016/j.neuroscience.2011.04.051.
Petrov, A.M., Yakovleva, A.A., Zefirov, A.L., 2014 Nov 15. Role of membrane cholesterol in spontaneous exocytosis at frog neuromuscular synapses: reactive oxygen species-calcium interplay. J. Physiol. 592 (22), 4995–5009. http://dx.doi.org/10.1113/jphysiol.2014.279695. (Epub 2014 Oct 17).
Pye, D., Palomero, J., Kabayo, T., Jackson, M.J., 2007. Real-time measurement of nitric oxide in single mature mouse skeletal muscle fibres during contractions. J. Physiol. 581 (Pt 1), 309–318.
Reid, B., Slater, C.R., Bewick, G.S., 1999. Synaptic vesicle dynamics in rat fast and slow motor nerve terminals. J. Neurosci. 19 (7), 2511–2521.
Rizzoli, S.O., Betz, W.J., 2005. Synaptic vesicle pools. Nat. Rev. Neurosci. 6 (1), 57–69.
Rocha, M.C., Pousinha, P.A., Correia, A.M., Sebastião, A.M., Ribeiro, J.A., 2013. Early changes of neuromuscular transmission in the SOD1(G93A) mice model of ALS start long before motor symptoms onset. PLoS One 8, e73846. http://dx.doi.org/10.1371/journal.pone.0073846.
Rodrigues, H.A., Lima, R.F., Fonseca Mde, C., Amaral, E.A., Martinelli, P.M., Naves, L.A., Gomez, M.V., Kushmerick, C., Prado, M.A., Guatimosim, C., 2013. Membrane cholesterol regulates different modes of synaptic vesicle release and retrieval at the frog neuromuscular junction. Eur. J. Neurosci. 38 (7), 2978–2987. http://dx.doi.org/10.1111/ejn.12300.
Sasaki, S., Shibata, N., Iwata, M., 2001. Neuronal nitric oxide synthase immunoreactivity in the spinal cord in amyotrophic lateral sclerosis. Acta Neuropathol. 101 (4), 351–357.
Shafaati, M., Mast, N., Beck, O., Nayef, R., Heo, G.Y., Björkhem-Bergman, L., Lütjohann, D., Björkhem, I., Pikuleva, I.A., 2010. The antifungal drug voriconazole is an efficient inhibitor of brain cholesterol 24S-hydroxylase in vitro and in vivo. J. Lipid Res. 51 (2), 318–323. http://dx.doi.org/10.1194/jlr.M900174-JLR200.
Slater, C.R., 2015. The functional organization of motor nerve terminals. Prog. Neurobiol. 134, 55–103. http://dx.doi.org/10.1016/j.pneurobio.2015.09.004.
Sugita, S., Fleming, L.L., Wood, C., Vaughan, S.K., Gomes, M.P., Camargo, W., Naves, L.A., Prado, V.F., Prado, M.A., Guatimosim, C., Valdez, G., 2016. VAChT overexpression increases acetylcholine at the synaptic cleft and accelerates aging of neuromuscular junctions. Skelet. Muscle 6, 31. http://dx.doi.org/10.1186/s13395-016-0105-7.
Sun, M.Y., Taylor, A., Zorumski, C.F., Mennerick, S., 2017. 24S-hydroxycholesterol and 25-hydroxycholesterol differentially impact hippocampal neuronal survival following oxygen-glucose deprivation. PLoS One 12 (3), e0174416. http://dx.doi.org/10.1371/journal.pone.0174416.
Sunico, C.R., Domínguez, G., García-Verdugo, J.M., Osta, R., Montero, F., Moreno-López, B., 2011. Reduction in the motoneuron inhibitory/excitatory synaptic ratio in an early-symptomatic mouse model of amyotrophic lateral sclerosis. Brain Pathol. 21 (1), 1–15. http://dx.doi.org/10.1111/j.1750-3639.2010.00417.x.
Sural-Fehr, T., Bongarzone, E.R., 2016. How membrane dysfunction influences neuronal survival pathways in sphingolipid storage disorders. J. Neurosci. Res. 94 (11), 1042–1048. http://dx.doi.org/10.1002/jnr.23763.
Teixeira, G., Vieira, L.B., Gomez, M.V., Guatimosim, C., 2012. Cholesterol as a key player in the balance of evoked and spontaneous glutamate release in rat brain cortical synaptosomes. Neurochem. Int. 61 (7), 1151–1159. http://dx.doi.org/10.1016/j.neuint.2012.08.008.
Thomas, S., Robitaille, R., 2001. Differential frequency-dependent regulation of transmitter release by endogenous nitric oxide at the amphibian neuromuscular synapse. J. Neurosci. 21 (4), 1087–1095.
Tremblay, E., Martineau, É., Robitaille, R., 2017. Opposite synaptic alterations at the neuromuscular junction in an ALS mouse model: when motor units matter. J. Neurosci. 37 (37), 8901–8918. http://dx.doi.org/10.1523/JNEUROSCI.3090-16.2017.
Trias, E., Ibarburu, S., Barreto-Núñez, R., Varela, V., Moura, I.C., Dubreuil, P., Hermine, O., Beckman, J.S., Barbeito, L., 2017. Evidence for mast cells contributing to neuromuscular pathology in an inherited model of ALS. JCI Insight. 2 (20). http://dx.doi.org/10.1172/jci.insight.95934.
Uchitel, O.D., Scornik, F., Protti, D.A., Fumberg, C.G., Alvarez, V., Appel, S.H., 1992. Long-term neuromuscular dysfunction produced by passive transfer of amyotrophic lateral sclerosis immunoglobulins. Neurology 42 (11), 2175–2180.
Ullrich, C., Pirchl, M., Humpel, C., 2010. Effects of cholesterol and its 24S-OH and 25-OH oxysterols on choline acetyltransferase-positive neurons in brain slices. Pharmacology 86 (1), 15–21. http://dx.doi.org/10.1159/000314333.
Venturini, G., Colasanti, M., Fioravanti, E., Bianchini, A., Ascenzi, P., 1999. Direct effect of temperature on the catalytic activity of nitric oxide synthases types I, II, and III. Nitric Oxide 3 (5), 375–382.
Wuolikainen, A., Acimovic, J., Lövgren-Sandblom, A., Parini, P., Andersen, P.M., Björkhem, I., 2014. Cholesterol, oxysterol, triglyceride, and coenzyme Q homeostasis in ALS. Evidence against the hypothesis that elevated 27-hydroxycholesterol is a pathogenic factor. PLoS One 9 (11), e113619. http://dx.doi.org/10.1371/journal.

pone.0113619.
Zamir, O., Charlton, M.P., 2006. Cholesterol and synaptic transmitter release at crayfish neuromuscular junctions. J. Physiol. 571 (Pt 1), 83–99.
Zheng, Z., Sheng, L., Shang, H., 2013. Statins and ALS: a systematic review and meta-analysis. Amyotroph. Lateral Scler. Frontotemporal Degener. 14, 241–255.
Zhu, H., Bhattacharyya, B., Lin, H., Gomez, C.M., 2013. Skeletal muscle calpain acts through nitric oxide and neural miRNAs to regulate acetylcholine release in motor nerve terminals. J. Neurosci. 33 (17), 7308–7324. http://dx.doi.org/10.1523/JNEUROSCI.0224-13.2013.
Zidovetzki, R., Levitan, I., 2007. Use of cyclodextrins to manipulate plasma membrane cholesterol content: evidence, misconceptions and control strategies. Biochim. Biophys. Acta 1768 (6), 1311–1324.